Chapter 2

Theoretical background

The first part of this chapter gives an overview of the main static magnetic behavior of itinerant ferromagnetic and antiferromagnetic materials. The formation of the magnetic order is described. A more detailed discussion focuses on ferromagnetic systems in direct contact to antiferromagnets.

In this work, spin-polarized scanning tunneling microscopy (Sp-STM) is used to investigate the local magnetic structure at sample surfaces. The basic principles of this technique are summarized in the second part of this chapter.

2.1 Itinerant ferromagnets and antiferromagnets

Ferromagnetic and antiferromagnetic solids are characterized by magnetic moments which show magnetic order below a critical temperature. For ferromagnets this ordering temperature is called Curie-temperature (T_C) and for antiferromagnets Néel-temperature (T_N). The spontaneous order of the magnetic moments is caused by an interaction between them. The ferromagnets Fe, Co, Ni and antiferromagnets Cr and Mn are 3d metals, in which itinerant electrons carry the magnetic moments. In these materials, the magnetic moments are mainly caused by the electron spin. The orbital magnetic moments are quenched because of a strong inhomogeneous electrical field in these crystals [36]. The strongest interaction, which is responsible for the magnetic order, is the exchange interaction. This interaction results from the quantum mechanical properties of the indistinguishability of the electrons, but the origin is the electrostatic Coulomb interaction.

In the Heisenberg model [37], the Hamiltonian describes the exchange interaction of localized magnetic moments. In the case that the total magnetic moment is dominated by the moments of the electron spins, the Hamiltonian can be expressed by:

$$H = -\frac{1}{2} \sum_{i,j \neq i} J_{ij} \overrightarrow{S}_i \cdot \overrightarrow{S}_j \tag{2.1}$$

where $\overrightarrow{S}_{i(j)}$ is the total spin moment of the atom at the position $i(j)$. J_{ij} is the

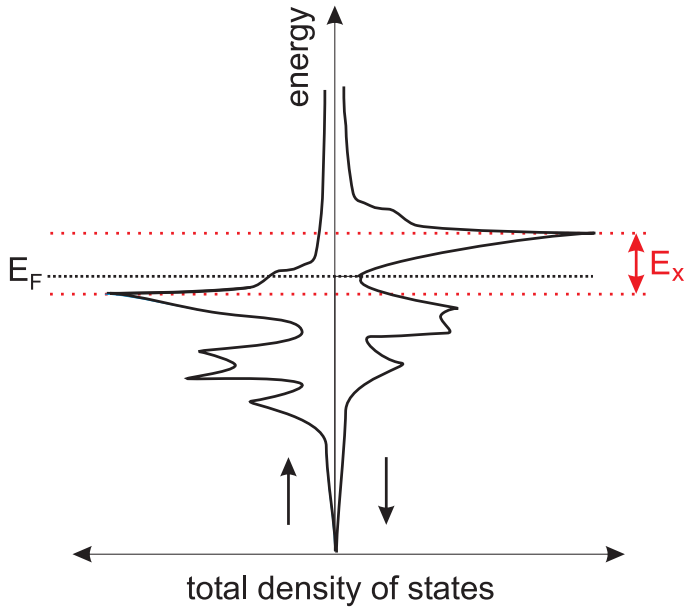

Figure 2.1: Total density of states of bulk Fe showing the exchange splitting by the amount E_x between majority electrons (↑) and minority electrons (↓) [42]. The Fermi energy is indicated by E_F.

exchange coupling constant between particular magnetic moments. When the sign of J_{ij} is positive the lowest energy is reached for parallel alignment of spins, which means ferromagnetic order is preferred. For negative sign, the spins do not couple parallel so that the total magnetic moment vanishes. Antiferromagnetic order is preferred. For a detailed description see for example [38]. Later (in section 5.1.2), a Heisenberg model is used to model the micromagnetic behavior of the system under investigation.

In 3d metals, the itinerant electrons are not localized but arranged in bands. The magnetic order in these materials was discussed by Stoner [39,40]. The requirement for ferromagnetism, i.e. the Stoner criterium, is that the product of the density of states at the Fermi energy and the exchange interaction is larger than a critical value. For details see for example Ref. [41]. If the Stoner criterium is fulfilled, a splitting of the bands for spin up and spin down electrons occurs and due to the fact that the Fermi energy for both spin directions has to be the same a difference in the occupation for spin up and spin down electrons is caused. Such a situation is present in the 3d ferromagnetic metals Fe, Co and Ni. In these metals, the bands are exchange split and the summation over all occupied states yields a greater number of so-called majority electrons than of minority electrons resulting in a net magnetic moment. Fig. 2.1 shows the spin-polarized density of states of bcc Fe which arises by integrating over all states having different wave vectors but the same energy. The exchange splitting between the bands is indicated by the energy E_x. Because of the exchange splitting, the occupation for majority and minority electrons close to the

Fermi level is different resulting in a spin polarization of the conduction electrons. The spin polarization at the Fermi energy is given by the density of states at this energy. The spin polarization close to the Fermi level is an important quantity in this work because this property is used in Sp-STM, as will be shown later (see section 2.3).

The difference between ferromagnetism and antiferromagnetism is the absence of a net magnetic moment in one magnetic unit cell, in the latter case. Different types of antiferromagnetic order exist and one special case is the antiparallel coupling of neighboring magnetic moments. When introducing a surface along specific crystallographic directions in these antiferromagnets, the neighboring antiferromagnetic order can result in uncompensated surfaces. In this case, the neighboring magnetic moments within one layer are coupled ferromagnetically but antiferromagnetically to adjacent layers. Thus, the net magnetic moment of each separate monolayer (ML) is non zero. These types of antiferromagnets are called layer-wise antiferromagnets. Examples are NiO(111) [43], Cr(001) [5], Cr/Fe(001) [44,45] and Mn/Fe(001) [46,47]. In this work, the uncompensated surfaces of the layer-wise antiferromagnetic ordered films of Mn/Fe(001) and Cr/Fe(001) are studied by Sp-STM.

2.1.1 Domains and domain walls

In a magnetic material, the magnetization prefers to lie along certain crystallographic directions, the so-called easy axes. This is caused by the magneto-crystalline anisotropy.

A magnetic particle having a net magnetization has magnetic poles producing magnetic surface charges. These charges result in a magnetic stray field containing magnetic energy which is energetically unfavorable. The reduction of the stray field energy is achieved by aligning the magnetic moments parallel to the particle boundary to obtain a magnetic closed flux.

A direct consequence of these energy contributions is that the magnetic order in a ferromagnetic particle may split up into domains. Within the domains, the magnetic moments are pointing in one direction. In different domains they are often aligned along different easy axes [48]. A continuous transition between adjacent domains is formed by domain walls. Two different kinds of domain walls exist: Bloch walls, where the magnetization rotates in the plane of the wall and Néel walls, where the magnetization rotates perpendicular to the plane of the wall. The width of natural bulk domain walls is determined by the competition between the anisotropy and the exchange energy. The exchange alone would result in an infinitely wide wall, where the angle between neighboring magnetic moments is infinitesimal small, whereas the anisotropy would prefer an atomically sharp transition.

By using a magnetic continuum model, the width of static domain walls can be calculated. In this model, the magnetization is taken as a continuum in space and the atomistic discretization is neglected. This model is naturally limited to large structures, where atomistic details are not important. In general, there are

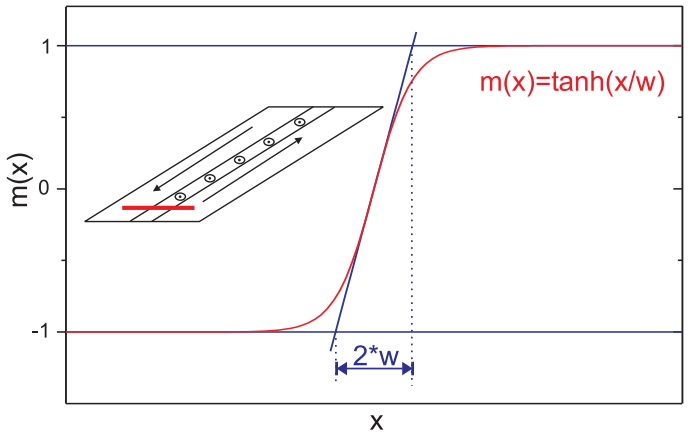

Figure 2.2: A magnetic line profile calculated for a 180° bulk wall. The line profile is a *tanh*-function and the width of the domain wall is given by $2w$. In the inset, the underlying magnetic configuration is shown.

no analytical solutions for the equilibrium magnetic structure in three dimensions when considering all energetic terms. However, an analytical solution can be found for the wall profile in a one-dimensional 180° domain wall when considering only the magneto-crystalline anisotropy and the exchange interaction and neglecting the stray field [48]. The resulting profile is a simple *tanh*-function

$$m(x) \propto tanh(x/w). \tag{2.2}$$

Here, $m(x)$ is the normalized projection of the magnetization along the direction perpendicular to the domain wall (along the red line in the inset of Fig. 2.2). The domain wall width ($2w$) is defined by the crossings of the tangent at $m(0)$ with the saturation lines, see Fig. 2.2. Throughout this work, the *tanh*-function is used to determine wall widths between two domains. For a 180° Bloch wall the width is given by

$$w = 2\sqrt{A/K} \tag{2.3}$$

where K is the anisotropy constant and A is the exchange constant [48]. By considering the lattice constant a of the crystal, J and A are related by:

$$A = \frac{JS^2}{a}c \tag{2.4}$$

where c =1, 2 or 4 for a simple cubic, bcc or fcc crystal structure, respectively [38].

For thick films or in bulk crystals, typically Bloch walls are formed as these walls are free of magnetic charges. At the surface, Bloch walls produce magnetic charges and thus create a stray field. Néel walls are not charge free in the interior of the wall. They, however, produce no charges at the sample surface. Therefore, Néel walls are often energetically more favorable at surfaces and in thin films [48]. To minimize the energy of bulk walls, the direction of rotation of the magnetization near the

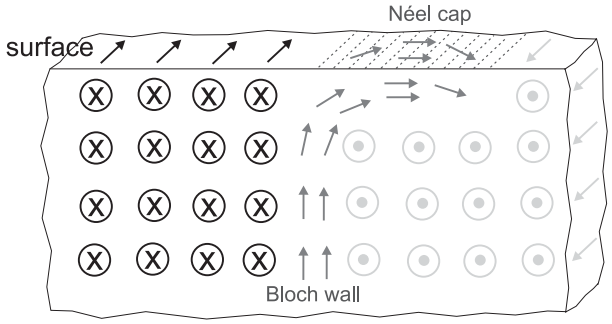

Figure 2.3: Schematic representation of the transition between a bulk Bloch wall and a surface Néel wall. The Bloch wall is running vertically through the center of the image and is terminated into a Néel cap at the surface. Crosses and dots correspond to magnetization vectors pointing in and out of the image plane.

surface can turn over from a rotation parallel to the plane of the domain wall to a rotation perpendicular to it. In other words, to reduce the magnetic charges a bulk Bloch wall can terminate in a Néel wall at the sample surface [49]. Fig. 2.3 shows a schematic sketch where a Bloch wall is transformed into a Néel wall at the surface.

Domains in antiferromagnets are defined as areas showing the same order of magnetic moments. In ferromagnets the driving force for creating domains is the stray field. Due to the absence of macroscopic stray fields in antiferromagnets, other mechanisms have to be responsible for the formation of domains. Perturbations of the regular arrangement of the crystal lattice may disturb the antiferromagnetic order. Recently, antiferromagnetic domains were imaged on $LaFeO_3$ [50, 51] showing that the domain structure can be correlated to areas of different crystallographic order (crystallographic domains). In a different work, antiferromagnetic domains were imaged in NiO single crystals. In this case, the formation of domains is attributed to magneto elastic effects [52–54].

Locale defects in a crystal, e.g. screw dislocations, can cause the formation of domains [5]. As shown in the present work, another defect, i.e. monatomic steps at an interface between a ferromagnetic substrate and an antiferromagnetic film, also lead to the formation of domains in the antiferromagnet.

2.1.2 Exchange coupled systems: an uncompensated antiferromagnet in contact to a ferromagnet

A ferromagnet in direct contact to an antiferromagnet is called an exchange coupled system. In the following, we will only consider uncompensated antiferromagnets of such an exchange coupled system. Complex effects can occur caused by the exchange interaction at the interface between a ferromagnet and an antiferromagnet. The most common structural defects at the interface are monatomic steps. When a layer-wise antiferromagnetic film is overgrowing monatomic steps of a ferromagnetic

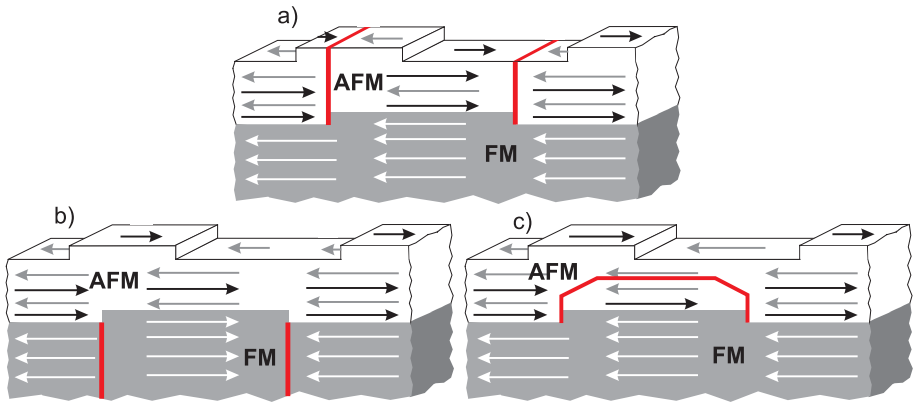

Figure 2.4: Three possible structures of magnetic frustrations caused by monatomic steps at the interface between a layer-wise antiferromagnet and a ferromagnet. In a) the magnetic frustration is formed throughout the antiferromagnetic film above the buried substrate steps and in b) the frustration is formed in the substrate. c) shows the possibility of forming a closed magnetic frustration within the antiferromagnetic layer connecting two frustrated regions. This frustration could also be formed at the interface or in the substrate.

substrate, a difference in the thickness of one atomic layer between both sides of the steps is created in the film. In the case of collinear coupling between the antiferromagnet and the ferromagnet, it is not possible to keep for all nearest neighbors the ferromagnetic order in the ferromagnet, the antiferromagnetic order in the antiferromagnet, and the same magnetic order at the interface. This conflict in the magnetic order leads to a magnetic frustration. Three possible configurations for a magnetic frustration are illustrated in Fig. 2.4. In the configuration of Fig. 2.4a) and b) either the antiferromagnet or the ferromagnet is split into two domains at each position of an interface step. The magnetic frustration starts at the step edges and is located above or below them throughout the film. In the third case (Fig. 2.4c), a magnetic defect line is formed parallel to the interface connecting two frustrations at interface steps. The wall can either lie in the ferromagnet or the antiferromagnet or at the interface. The region of magnetic frustration caused by such defect lines is often described as a domain wall caused by a frustration [55–57]. Close to the topological defect, the magnetically frustrated region cannot be described by a competition between the exchange and the anisotropy energy as in the case of conventional domain walls in ferromagnets and antiferromagnets (section 2.1.1). The magnetic frustration is pinned at this topological perturbation. The main focus of this work lies on the investigation of magnetic frustrations in thin antiferromagnetic films caused by monatomic steps at the interface in an exchange coupled system. In the following, an overview of models and calculations performed on these kind of magnetic frustrations is given.

Berger and coworkers [56] performed calculations of a model system consisting of

a ferromagnetic film on top of a bulk antiferromagnet having two monatomic steps at the interface. Note that this is the reversed situation compared to the one shown in Fig. 2.4. They found the three phases of wall states illustrated in the figure. In their calculations, it was demonstrated that the stability of each phase depends on the over-layer thickness, the defect density, the strength of the exchange coupling and the temperature [56]. In the special case that the temperature is well below T_C and T_N and in the limit of low step density, it is energetically more favorable to form magnetic frustrations in the thin over-layer (case Fig. 2.4a)). In the case of a high step density at the interface, magnetic frustrations can be connected to reduce the length of the magnetic frustration and thus the energy of the system, as illustrated in Fig. 2.4c) [58].

Morosov and coworkers [57, 59] performed calculations for a thin antiferromagnetic film on top of a much thicker ferromagnetic substrate having monatomic steps at the interface. Their calculations show the formation of a wall in the thin film separating it into domains of opposite magnetization directions. This behavior was observed assuming similar conditions as used by Berger and coworkers [56] for the case that the magnetic frustration was formed in the thin over-layer. Their calculations correspond to the case presented in Fig. 2.4a). For such a situation, it was shown that the main rotation of spins occurs in the thin film and that only a small tilt of the spins is present in the ferromagnetic substrate. In the limit of thin films, the width of the created magnetic frustration was found to be smaller than the width of conventional domain walls and it is mainly determined by a competition between different exchange interactions in the ferromagnetic-antiferromagnetic system [57, 59].

The most frequently studied system in this context is Cr on Fe [55, 60–63]. Stoeffler and coworkers [62,63] studied the magnetic behavior of Cr atoms on a stepped Fe substrate. Thin Cr films on Fe (001) show a layer-wise antiferromagnet coupling [44, 45]. Therefore, this system is a realization of the model described in Fig. 2.4. The calculations show the formation of a magnetic frustration in the form of a defect line separating two Cr domains of opposite magnetization at the position of the Fe substrate step, corresponding to the case a) in Fig. 2.4. The calculations indicate a rotation and a change of the size of the magnetic moments in the antiferromagnetic film above an Fe step edge. Also a tilt of the magnetic moments of the underlying Fe substrate in the vicinity of the step edge was found. The magnetically frustrated region increases in width with increasing the Cr thickness. The lateral extension of the magnetic frustration is rather small, only extended over some atoms, and localized in the vicinity of the Fe step. The magnetic configuration at the surface reflects the roughness of the Cr surface and the interface roughness between Cr and Fe. As we will see later, the behavior of the magnetic frustration theoretically predicted for the system Cr on Fe is found experimentally for a similar system, layer-wise antiferromagnetic ordered Mn films on Fe(001).

2.2 Tunneling and scanning tunneling microscopy

Since the development of quantum mechanics in the 1920s, it is known that a particle with a kinetic energy smaller than the potential energy of a barrier has a non-vanishing probability to enter the barrier. In the case of a finite potential barrier (height and width), the particle can tunnel from one side of the barrier to the other one. When the tunneling particles are charged, e.g. electrons, this results in a so-called tunneling current. In a one dimensional model with a rectangular potential barrier (V_B) and for free electrons with a kinetic energy $E < V_B$ the solution of the Schrödinger equation gives a simple correlation between the tunneling current and the barrier width (d):

$$I \propto e^{-2kd} \tag{2.5}$$

with the wave vector $k = \sqrt{2m(V_B - E)}/\hbar$. Here, m is the electron mass, and $\hbar$ the Planck constant divided by 2π. As a result, the tunneling current decays exponentially with increasing barrier width due to the exponential decay of the probability density of the electrons in the barrier. The tunneling probability from each side of the barrier to the opposite side is the same. Therefore, the resulting tunneling current is zero. When a voltage is applied over a barrier (between two electrodes) their Fermi energies are shifted with respect to each other and a net tunneling current flows. In materials, a barrier exists which electrons need to overcome to enter the vacuum. It is the energetic difference between the bound states and states in the vacuum and is called work-function.

The high sensitivity of the tunneling current on the distance is used in scanning tunneling microscopy (STM). There, one electrode is replaced by a conducting tip which is scanned over a sample surface, while the local tunneling current between the tip and the sample is measured. For this geometry and assuming the simple equation 2.5, one expects that electrons with a wave vector perpendicular to the sample surface yields the highest tunneling probability, while electrons with a component parallel to the surface have to travel a longer distance d which results in a reduced tunneling probability.

Typically, the work-function in metals have values of $4 - 5$ eV. Assuming the simple equation 2.5 and considering usual conditions of a STM experiment, a drop of the tunneling current by about one order of magnitude for every 1 Å of vacuum between the electrodes occurs.

The analysis of the local tunneling current in STM measurements opened the possibility to image electronic structures on a surface at the atomic scale [26]. The precise lateral and vertical movement of the tip during the scanning process in STM measurements is controlled by piezoelectrical crystals. These piezos change their length when a voltage is applied and the elongation can be precisely varied in the sub-angstrom range. The most common mode for performing STM measurements is the constant current mode (Fig. 2.5). In this case, the tip is stabilized at a fixed voltage (of the order of 1 V) applied between tip and sample and a fixed tunneling current (typically of the order of 1 nA) above the sample surface. Holding the

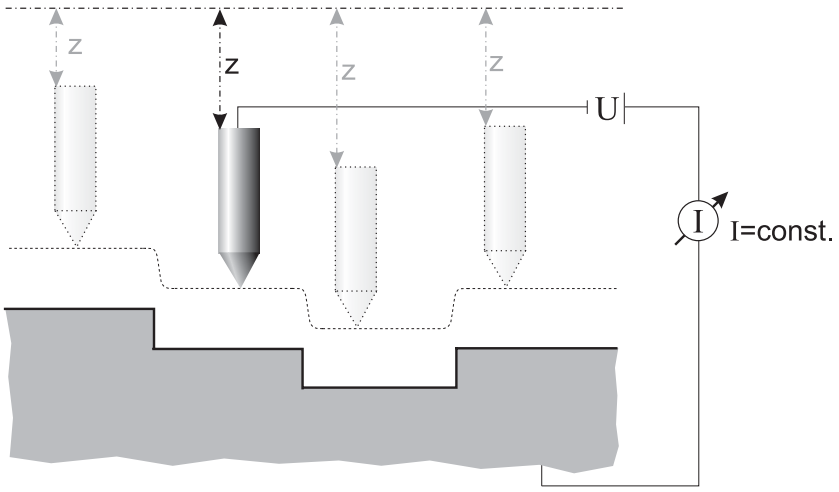

Figure 2.5: Schematic drawing of a STM working in a constant current mode. While the tip is scanned over the sample surface, the tunneling current is kept constant by changing the vertical position of the tip (indicated by the length z).

tunneling current and the bias voltage constant the tip is scanned over the sample surface while the vertical position of the tip is adjusted by a piezoelectrical feedback mechanism. Thus, the tip is following the contour lines of constant tunneling current, as indicated by the dashed line in Fig. 2.5. By detecting the vertical motion of the piezo, a contour map of the constant tunneling current of a sample surface is obtained. For details see for example Ref. [64]

To describe the features visible in STM images, the transmission probability between the tip and the sample has to be known. This requires the knowledge of the atomic structure of the tip and the sample surface. One of the notorious problems is the unknown and noncontrollable detailed arrangement of the atoms at the end of a STM tip. In the approach of Tersoff and Hamann [65, 66], the atomistic arrangement of the atoms at the tip apex is assumed to be spherical and characterized by a spherical potential well. The electronic structure of the tip is considered to be constant and described by a s-orbital. Using these simplifications, they found that the tunneling current is proportional to the density of states of the sample at the position of the tip apex which is described by the center of the sphere $\vec{R}$. Thus, in this model STM images present only properties of the sample surface. In the limit of small voltages ($eV \ll \phi$, with ϕ being the work-function) the tunneling current (I) can be written as:

$$I \propto eV n^s(\vec{R}, E_F) \tag{2.6}$$

where $n^s(\vec{R}, E_F)$ is the local density of states of the sample surface at the position $\vec{R}$. $n^s(\vec{R}, E_F)$ includes the wave function of the sample at the position $\vec{R}$ and the exponential decay of the wave function within the vacuum gap. In this description, an image of constant tunneling current presents a plane of constant local density

of states of the sample surface. In this case and a homogeneous sample, in first approximation constant tunneling current images reflect the topography of a sample surface.

In the Tersoff and Hamann model, the lateral resolution of the STM (δ) is determined by the radius of the sphere placed at the tip apex, the distance between tip and sample (d), and the wave vector of the tunneling electrons, $\delta = [2k^{-1}(R+d)]^{1/2}$ [65]. As a result, the measured structure (w_{exp}) can be treated as a superposition of two Gaussian functions consisting of the local expansion of the surface structure (w_s) and the resolution of the STM tip $w_{exp} = \sqrt{w_s^2 + \delta^2}$. Since the tip apex is always finite and cannot be smaller than one atom, monatomic steps can never be imaged atomically sharp, as indicated in Fig. 2.5.

In scanning tunneling spectroscopy (STS) measurements, the tip is scanned over the sample surface (as in normal STM measurements) and at each scanning position, the tip to sample distance is fixed for a short moment while the bias voltage is ramped. Therefore, variations of the tunneling current as a function of the bias voltage (U) are measured, resulting in I/U spectra of each spatial point. Within the simple Tersoff and Hamann model, the differential conductivity dI/dU is directly proportional to the local density of states of the sample surface. One possibility to measure directly dI/dU spectra is to apply a small alternating voltage on top of the ramped bias voltage. By detecting variations of dI/dU as a function of the bias voltage, the local electronic properties can be observed. Thus, the dispersion of bulk states, resonances and surface states can be visualized [67]. Surface states are characterized by spatial localization of electron states at the surface. The bands of surface states are placed in the energy gap of bulk bands. If a band of a surface state is overlapping with a bulk band, the resulting state is called resonance due to imperfect localization at the surface [68].

The simple interpretation of treating the STM images as the topography of the sample surface has to be taken with caution. The tunneling current depends in a complex way on the electronic structure which is especially important on the atomic scale. In the nanometer range or at larger scales, however, the interpretation of STM images as the topography can be a good approximation. An overview of the interpretation of STM images based on the above mentioned theory is given in Ref [69].

A more complete model of STM images, including the dependence of changes of the tunneling current with the bias voltage, requires a complete description of the electronic structure of the sample, the tip and the coupling between them through the vacuum gap. The Landauer-Büttiker theory [70], which is introduced in the context of spin-polarized tunneling in the following section, is one step in this direction.

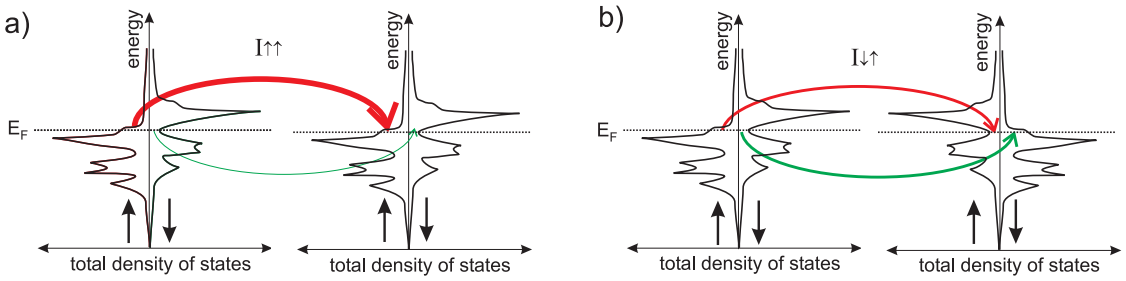

Figure 2.6: Simple illustration of the origin of the spin-dependent tunneling current on the example of the bcc Fe spin-dependent density of states in the limit of small bias voltages. a) and b) show the case of parallel and antiparallel alignment of the magnetization of two Fe electrodes, respectively.

2.3 Spin-polarized scanning tunneling microscopy

First experiments on spin polarized tunneling where performed by spin-polarized field emission of electrons emitted from a magnetic tip [71,72]. In these experiments, a high negative voltage is applied to a sharp tip. The spin direction of the emitted electrons reflects the spin polarization of the material under investigation.

In 1975 Jullière discovered that the tunneling current between two ferromagnetic electrodes separated by an insulator depends on the relative orientation of the magnetization of both electrodes [28]. This effect is known as the tunneling magnetoresistance effect. In this experiment, one has to take into account not only the spin dependence of the occupied states in one electrode, as in the field emission experiments but also the one of the unoccupied states in the second electrode. Jullière proposed an explanation of his experimental result based on the spin polarization of the conduction electrons in both ferromagnetic electrodes. In his model, he assumed that the tunneling probability from any occupied state of one electrode to any unoccupied state in the other electrode is the same and that the tunneling current is independent of the geometry and the electronic structure of the barrier. Further assumptions are the conservation of the electron spin during the tunneling process, zero temperature (T=0 K), and a small external voltage. Under these conditions, the spin-dependent tunneling process can be explained by the difference in the spin-dependent densities of states at the Fermi energy. As already mentioned in section 2.1, the electron density in ferromagnetic materials at the Fermi energy is dominated by electrons with one particular spin direction resulting in a spin polarization close to the Fermi energy. Fig. 2.6 shows the spin-resolved density of states for two bcc Fe electrodes [42] having parallel (a)) or antiparallel (b)) alignment of their magnetization directions. At the Fermi energy there are more occupied and unoccupied states of majority than of minority character. The spin polarization close to the Fermi energy in Fe is about 35% [73]. In the case of parallel alignment of the magnetization of two Fe-electrodes, majority electrons from one electrode can tunnel into empty majority states of the other electrode and in an analogue way

minority electrons into minority states. If the magnetization direction of both Fe electrodes is aligned antiparallel, electrons having the same spin direction are of majority character in one electrode and of minority character in the other electrode. Because the electron spin is assumed to be conserved during tunneling, a different tunneling current flows for parallel and antiparallel alignment of the magnetization directions of the two Fe electrodes. Though, many simplifications are included in this model, it leads to a qualitative description of the spin-polarized tunneling process.

A more elaborate model by Slonczewski [74] shows that the tunneling current does not only depend on the properties of the ferromagnetic electrodes but as well on the electronic structure of the tunneling barrier. He analyzed the tunneling current through a rectangular barrier by assuming that the tunneling electrons in the two ferromagnets are free electrons. Therefore, he described the ferromagnets by two simple parabolic bands (one for spin up and one for spin down) which are split by the exchange splitting. Further assumptions included in his model are zero temperature (T=0K), vanishing external voltage, and that mainly electrons with a wave vector perpendicular to the plane of the tunneling contact contribute to the tunneling process. The resulting equation for the spin-dependent tunneling current is given by:

$$I = I_0(1 + P_1 P_2 \cos\Theta), \tag{2.7}$$

where I_0 presents the tunneling current without spin polarization of the electrodes, $P_{1,2}$ is the effective spin polarization, and Θ is the angle between the magnetization directions of both ferromagnetic electrodes. The effective spin polarization is given by

$$P_{1,2} = \frac{k_{1,2}^{\uparrow} - k_{1,2}^{\downarrow}}{k_{1,2}^{\uparrow} + k_{1,2}^{\downarrow}} \cdot \frac{\kappa^2 - k_{1,2}^{\uparrow} k_{1,2}^{\downarrow}}{\kappa^2 + k_{1,2}^{\uparrow} k_{1,2}^{\downarrow}}. \tag{2.8}$$

Here, κ is the wave vector in the barrier[1] and $k_{1,2}^{\uparrow}, k_{1,2}^{\downarrow}$ are wave vectors of majority and minority electrons at the Fermi energy. In the free-electron model, $k^{\uparrow,(\downarrow)} \propto D^{\uparrow,(\downarrow)}(E_F)$ with $D(E_F)$ density of states at the Fermi energy. The first term of the effective spin polarization in equation 2.8 contains only the polarization of the two ferromagnetic electrodes as introduced by Jullière. The second term can be treated as a correction term which contains the barrier height. For high barriers ($\kappa^2 \gg k_{1,2}^{\uparrow} k_{1,2}^{\downarrow}$), the value of the effective polarization reduces to Jullière's result [75]. Slonczewski's model shows that the tunneling current depends on the type of the tunneling barrier which therefore plays an important role in the tunneling process.

Recently, it was possible to describe tunneling processes by ab-initio calculations which are based on the Landauer-Büttiker formalism [76]. The Landauer-Büttiker theory [70] is an elastic and ballistic transport theory in which two electrodes and a tunneling barrier are considered. Here, elastic means that the energy of the electrons is conserved and ballistic transport that the phase coherence of the electrons is maintained from the point when they entering the tunnel system until they leave it.

[1] $\kappa\hbar = [2m(E_F - V_B)]^{1/2}$.

In this case, the tunneling is described by the transmission probability of electrons, considered as Bloch waves which are passing the whole tunnel system. The tunneling current (I) is expressed by:

$$I \propto T(E), \tag{2.9}$$

where the transmission T depends on details of the electronic structure of the tunneling system, e.g. the dispersion relation ($E(k)$) and the barrier properties. The Slonczewski model is a special case of the Landauer-Büttiker theory, in which the realistic band structure is replaced with a free electron band. The consideration of realistic band structures, obtained by ab-initio calculations and included in the Landauer-Büttiker theory, shows that the band gaps have a pronounced influence on the tunneling current. Thus, the different matching between the electronic states plays an essential role. However, a direct consequence of this transport approach is that localized states, e.g. surface states cannot contribute to the tunneling current because they are placed in energy band gaps of the bulk states and they have only a wave vector parallel to the sample surface. In contrast to surface states, resonances can couple to the bulk states and they can produce a strong enhancement of the tunneling current. Using the above introduced theory, the spin-dependent tunneling current through various tunnel systems has been calculated recently [77–82].

In Sp-STM measurements, the spin-dependent tunneling current is used to investigate the spin polarization of a sample surface in addition to the topography. The spin polarization gives information of the local magnetization of a sample surface. In a Sp-STM, the two ferromagnetic electrodes are replaced by a ferromagnetic STM electrode (tip or ring, as shown later) and a ferromagnetic sample and the vacuum between Sp-STM electrode and sample plays the role of the insulator [4]. As shown in equation 2.7, the spin-polarized tunneling current depends on the angle θ between both magnetization directions. Switching the magnetization (M) of the electrode from M to $-M$ corresponds to a change of the angle from θ to $\theta + 180°$. One can easily see that the average of the two spin depended tunneling currents reduces to $\bar{I} = I_0$. Therefore, the average tunneling current (averaged over the opposite alignment of the magnetized directions) is independent of the spin polarization and yields the topographic information like in the case a non magnetic electrode is used. However, the difference of these two spin-dependent tunneling currents is proportional to the spin polarization, $\Delta I = 2I_0P_1P_2\cos\Theta$.

The magnetization direction of the Sp-STM electrode defines the direction of sensitivity and hence the direction of the imaged component of the spin polarization of the sample surface (Fig. 2.7). Performing constant tunneling current STM measurements and using ferromagnetic STM electrodes which are magnetized in one direction, changes of the spin-polarized tunneling current will change the distance between electrode and sample surface. This is because the feedback mechanism will adjust the vertical position of the electrode to keep the tunneling current constant. A change of the spin polarization is only visible in the form of an additional topographic contrast in the STM image [30]. When the magnetization of the electrode is switched with a frequency much higher than the frequency of the feedback mecha-

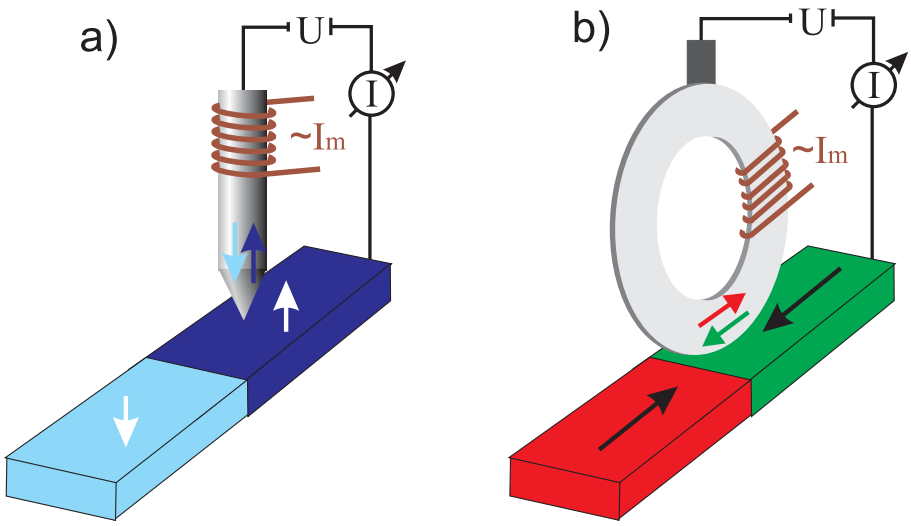

Figure 2.7: Schematic representation of Sp-STM electrodes, a) for measuring the out-of-plane [4] and b) the in-plane component [7].

nism, no changes of the distance occurs as the changes of the spin-polarized tunneling current are averaged out. Therefore, one can separate an average tunneling current $\bar{I}$ which gives topographic information from the modulated current ΔI that results from the spin-polarized tunneling current and yields the spin information.

In our experiment, the magnetization of a ferromagnetic STM electrode is switched by applying a small alternating current to a coil wound around the electrode. This is schematically shown in Fig. 2.7. The alternating magnetic field induced within the coil is large enough to fully reverse the magnetization of the electrode. Details of the experimental realization are described in section 3.1.1.

To measure the magnetic out-of-plane component, a sharp ferromagnetic tip is used. Using the above described technique, the out-of-plane magnetization component was imaged for the first time in 1998. A high lateral resolution of at least 1 nm has been achieved [35]. Because of the elongated shape of a sharp tip, it has a large shape anisotropy resulting in a magnetization direction collinear to the axis of the tip. The sharper the tip the smaller the amount of magnetic material close to the sample and hence the smaller the stray field which may influence the magnetization of a sample [83]. Fig. 2.7a) shows a schematic drawing of the out-of-plane setup.

In this work, the concept of the Sp-STM is expanded by the capability to image a well-defined in-plane component. To investigate the in-plane spin polarization of a sample surface a Sp-STM electrode is needed having a magnetization direction in the plane of a sample surface at its apex. Because of the above mentioned reason it is difficult to achieve in-plane sensitivity using a conventional sharp tip. One solution is to use a ferromagnetic ring (Fig. 2.7b)) as a Sp-STM electrode. Here, the magnetization direction lies always tangential to the outer perimeter of a ring. Thus, at the bottom of the ring where the tunneling occurs, the magnetization lies

in the plane of the sample surface. Because the magnetic flux in an ideal ring is closed, the magnetic stray field is zero. Therefore, ideal rings have no influence on the magnetization of the sample. By choosing the plane in which the ring is oriented, the magnetization direction of the ring is defined and thus the direction of the sensitivity in the surface plane for the measured spin signal is known as well. One may wonder if such macroscopic rings used as a STM electrode will not significantly decrease the lateral resolution. As it will be shown later, the rings are not perfectly smooth and nano tips exist at the apex which can give a high lateral resolution.

Besides the imaging of magnetic structures, Sp-STM measurements allow the investigation of the spin-dependent tunneling current through a well-defined tunneling barrier (vacuum gap). Under these well-defined conditions, one typical experimental difficulty of a structured three layer system, the undefined interfaces and thus complicated potential barriers, is avoided [80]. The size and sign of the spin-dependent tunneling current as a function of the bias voltage gives information of differences in the spin polarization close to the Fermi energy. Therefore, spin-polarized spectroscopic details can be obtained.

An other possibility to image the spin polarization of a sample surface by STM is to perform STS measurements [3]. In this case, non magnetic metal tips, e.g. W-tips, are coated with ferromagnetic or antiferromagnetic materials. Here, the magnetization of the tip is not switched during the measurements. Depending on the tip material and the material deposited on its apex, magnetic sensitivity is achieved for the in-plane or out-of-plane component [84]. Performing STS measurements dI/dU spectra are recorded and changes of the relative orientation between tip and sample magnetization may cause changes in the dI/dU spectra. In the case of a homogeneous electronic structure of the sample surface, these changes can be related to variations of the local magnetization at the sample surface. A typical dI/dU spectrum measured on an Fe (001) single crystal is presented in Fig. 2.8a) [1]. The spectra was taken with an Fe-coated W-tip being sensitive to the in-plane component of the spin polarization [3]. The peak in the spectra corresponds to the well known surface state at about 130 meV [85]. The difference in the spectra (solid and dotted lines) is caused by the fact that they were taken on oppositely magnetized domains on the Fe crystal. The largest difference in the dI/dU spectrum appears at the surface state, showing that it is strongly spin-polarized. Taking such dI/dU spectra by spatially scanning over the sample surface, images of one component of the local magnetization can be taken. Fig. 2.8b) presents a Sp-STS image of Fe islands on a pseudomorphic ML of Fe on W(110) [86]. The image shows the in-plane component of the magnetization. The dark and light islands are homogenously magnetized but the magnetization vector points in different directions.

When comparing Sp-STM with Sp-STS both methods have their advantages and their drawbacks. In the case of Sp-STM, changes of the spin polarization can clearly be separated from changes caused by spin-independent variations of the electronic structure. This allows the investigation of the spin polarization of sample surfaces having unknown and inhomogeneous electronic structures. In contrast, Sp-STS data

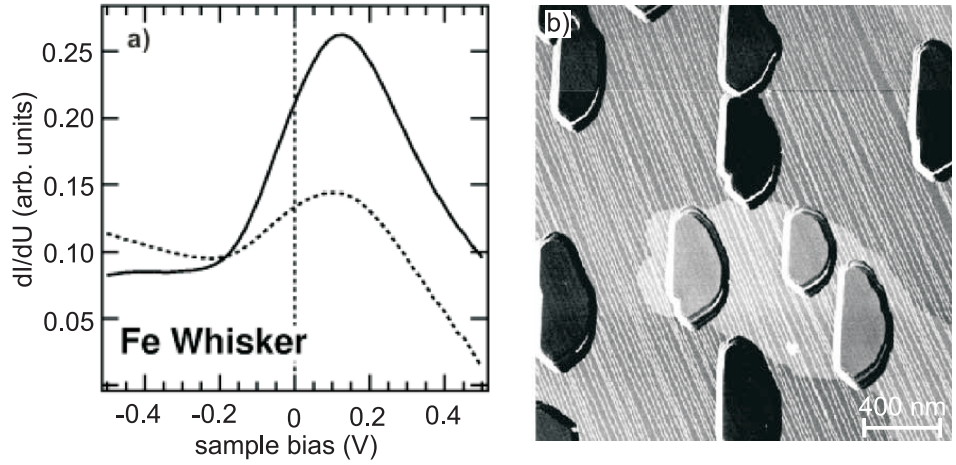

Figure 2.8: a) Sp-STS spectra (solid and dotted line) obtained on a clean Fe(001) surface by Yamasaki and coworkers [1]. The difference is caused by measuring on oppositely magnetized Fe domains. b) Sp-STS image of Fe islands on W(110) where each island is homogenously magnetized, but showing different orientations of their magnetization directions (black and gray islands), obtained by Bode and coworkers [86]. The two different gray levels of the surrounding correspond to different magnetization directions, as well. In these works, the in-plane magnetization component was imaged.

can only be interpreted as changes of the spin polarization of the sample surface when a homogenous electronic structure can be assumed. Since in Sp-STS the magnetization at the tip apex is fixed during scanning, the distance between tip and sample changes if the spin polarization of the sample surface changes. This leads to different tunneling conditions on different domains. This method is also only sensitive to variations of the spin-dependent tunneling current as a function of the bias voltage. A constant spin polarization cannot be detected because it would be compensated by changes of the tip to sample distance. In Sp-STM measurements, the distance between tip and sample is not changing on different magnetized domains (because the magnetization of the STM electrode is switched with a frequency that is higher than the frequency of the STM feedback loop), which allows the direct investigation of differences in the spin-polarized tunneling current. Using W-tips coated with an antiferromagnetic material, the magnetic stray field nearly vanishes and Sp-STS measurements can be performed under an applied external magnetic field [84]. This is impossible for higher fields using Sp-STM due to the necessity of switching the magnetization of the Sp-STM electrode. In Sp-STS, the magnetization direction of coated tips lies randomly in the plane of the sample surface whereas a well-defined in-plane component of the sample spin polarization can be imaged with Sp-STM using a ring as a STM electrode. In this work, only Sp-STM measurements were performed.